Research Article

Cancer Immunology Research

# Radretumab Radioimmunotherapy in Patients with Brain Metastasis: A $^{124}$I-L19SIP Dosimetric PET Study

Gian Luca Poli[1], Claudia Bianchi[1], Giorgio Virotta[1], Anna Bettini[1], Renzo Moretti[1], Eveline Trachsel[3], Giuliano Elia[3], Leonardo Giovannoni[2], Dario Neri[4], and Andrea Bruno[1]

## Abstract

Radioimmunotherapy (RIT) with $^{131}$I-labeled L19SIP (radretumab; a small immunoprotein format antibody directed against the ED-B domain of fibronectin; ~80 kDa molecular weight) has been investigated in several clinical trials. Here, we describe the use of immuno-PET imaging with iodine-124 ($^{124}$I)–labeled L19SIP to predict doses delivered to tumor lesions and healthy organs by a subsequent radretumab RIT in patients with brain metastases from solid cancer. Bone marrow doses were evaluated both during the diagnostic phase and posttherapy, measuring activities in blood (germanium detector) and whole body (lanthanum bromide detector). Expected doses for radretumab administration (4,107 MBq/m$^2$) were calculated from data obtained after administration of an average of 167 MBq $^{124}$I-L19SIP to 6 patients. To assess lesion average doses, the positron emission tomography (PET) scanner was calibrated for the use of $^{124}$I with an International Electrotechnical Commission (IEC) Body Phantom and recovery coefficients were calculated. The average dose to bone red marrow was 0.21 Gy/GBq, with high correlation between provisional and actual posttherapy doses. Although the fraction of injected activity in normal organs was similar in different patients, the antibody uptake in the neoplastic lesions varied by as much as a factor of 60. Immuno-PET with $^{124}$I-labeled L19SIP offers significant advantages over conventional $^{131}$I imaging, in particular accuracy of dosimetric results. Furthermore, the study indicates that antibody uptake can be highly variable even in different lesions of the same patient and that immuno-PET procedures may guide product development with armed antibodies. *Cancer Immunol Res; 1(2); 134–43. ©2013 AACR.*

## Introduction

There is growing interest in the use of "armed" antibodies (i.e., antibodies serving as delivery vehicles for active payloads such as cytotoxic drugs, radionuclides, cytokines, or other immunologic mediators) for therapeutic applications in cancer and in inflammation (1–5). These pharmaceutical developments rely crucially on the antibody's ability to localize at sites of disease. Immuno-PET, a molecular imaging technique combining the high resolution and sensitivity of positron emission tomography (PET) and the selective localization of antibodies at their target *in vivo*, has profited from recent technical advances and the availability of Good Manufacturing Practice (GMP)–grade radionuclides, and might play an important role in the future both in cancer staging and tailoring of therapy (6–10).

PET tracers of choice include iodine-124 ($^{124}$I), zirconium-89, copper-64, and fluorine-18. Published clinical data in the immuno-PET field comprise a phase I trial using $^{124}$I-cG250 for preoperative characterization of clear-cell renal carcinoma and a dosimetry trial with $^{89}$Zr-labeled U36 antibody in patients with head and neck cancers (11, 12). Although radiometals (e.g., Zr and Cu) are attached via chelators, iodine can be coupled directly with the antibodies without impacting on its pharmacokinetic properties. As iodine might be cleaved from the protein complex upon internalization, the use of $^{124}$I is particularly attractive for noninternalizing antibodies (7, 8).

In addition to diagnostic purposes, immuno-PET can be envisaged as a dosimetric tool to predict the optimal doses to target lesions and healthy organs of a subsequent radioimmunotherapy (RIT) using the same antibody coupled with a therapeutic isotope (13–15). Here, we describe the use of immuno-PET with $^{124}$I-L19SIP to calculate provisional doses for radretumab ($^{131}$I-L19SIP) RIT in patients with multiple brain metastases.

**Authors' Affiliations:** [1]Azienda Ospedaliera Papa Giovanni XXIII, Bergamo; [2]Philogen S.p.A., Siena, Italy; [3]Philochem AG, Otelfingen; and [4]Department of Chemistry and Applied Biosciences, Institute of Pharmaceutical Sciences, ETH Zurich, Zurich, Switzerland

**Note:** Supplementary data for this article are available at Cancer Immunology Research Online (http://cancerimmunolres.aacrjournals.org/).

**Corresponding Authors:** Gian Luca Poli, Department of Medical Physics, Azienda Ospedaliera Papa Giovanni XXIII, Bergamo, Italy. Phone: 39-035-2674266; Fax: 39-035-2674798; E-mail: glpoli@hpg23.it; and Dario Neri, Department of Chemistry and Applied Biosciences, Institute of Pharmaceutical Sciences, ETH Zurich, Wolfgang-Pauli-Strasse 10, CH-8093 Zurich, Switzerland. Phone: 41-44-633-74-01; Fax: 41-44-633-13-58; E-mail: neri@pharma.ethz.ch

**doi:** 10.1158/2326-6066.CIR-13-0007

©2013 American Association for Cancer Research.

Downloaded from http://aacrjournals.org/cancerimmunolres/article-pdf/1/2/134/2342431/134.pdf by guest on 21 May 2022

In patients with solid tumors, who subsequently develop distant metastases, 20% to 40% of them have metastases in the brain. Treatment regimens, which lead to measurable survival benefit include complete surgical excision, chemotherapy (in testicular cancer, lymphomas, and small cell lung cancer; ref. 16), or stereotactic irradiation. However, surgical excision can only be carried out in patients with one or a few brain metastases. In patients with more than 5 cerebral lesions, the general applicability of this form of treatment is still debated (17–20).

For multiple brain metastases, whole brain irradiation and stereotactic radiosurgery are the only therapeutic measures currently available (21–25). Whole brain radiotherapy (WBRT) is usually delivered in 10 fractions of 3 Gy (total dose: 30 Gy; ref. 26). Higher doses are detrimental to normal brain tissues, causing mental and psychomotor dysfunctions. Unfortunately, WBRT with 30 Gy is insufficient to improve overall survival in patients with multiple brain metastases; however, it has been shown to prolong the symptom-free intervals and may relief some of the symptoms (21). Stereotactic radiosurgery processes, such as "gamma knife" have been shown to be safe and effective for upfront and salvage treatments in patients with 5 or more brain metastases (25).

The fully human antibody L19 has been shown to preferentially localize around tumor blood vessels while sparing normal tissues (27, 28). L19 targets an epitope contained in the extra-domain B (EDB) of fibronectin, a highly conserved fibronectin-type III domain, which can be inserted into the fibronectin molecule by alternative splicing of the fibronectin pre-mRNA. EDB-containing fibronectin molecules are present in the extracellular matrix surrounding newly formed blood vessels, for example, in solid tumors, but they are undetectable in almost all healthy adult tissues (with the exception of female reproductive organs). Almost all actively proliferating solid tumors and most hematologic malignancies depend on neoangiogenesis for their growth and metastatic spread; tissues from these cancers express various levels of EDB-containing fibronectin (29, 30).

Comparative analysis of the L19 antibody in scFv, full immunoglobulin G (IgG), and small immunoprotein (SIP) format identified L19SIP as the preferred format for RIT (27, 31–33). The molecular weight of L19-SIP in its nonreduced form is approximately 80 kDa. RIT with $^{131}$I-labeled L19SIP (radretumab) has been investigated in a phase I and a subsequent phase I/II dose-finding and efficacy study in patients with a variety of cancers, where $^{131}$I-L19SIP has shown excellent tolerability at radioactive doses as high as 7,400 MBq (200 mCi) with therapeutic benefit for some patients enrolled in the study (34, 35). This phase II proof-of-concept study (EudraCT no. 2009-013002-13) was designed to test the feasibility of a combined treatment with radioactively labeled antibody and external radiotherapy, and identify first signs of clinical activity in patients with brain metastases of solid primary tumors. The combination of RIT and external beam irradiation promises additive antitumor effects of 2 independent modalities while minimizing burden to the dose-limiting organs (bone red marrow and normal brain).

Patients were selected for RIT based on the selective uptake of L19SIP to the brain lesions upon administration of a mean $^{124}$I-L19SIP activity of 167 MBq (~3.3 mg of protein).

Patients exhibiting favorable tumor-targeting (brain lesion/normal brain activity concentration ratio > 4 at 24 hours postinfusion (p.i.) as defined by PET) and with a provisional dose to the bone red marrow less than 2 Gy, were then treated with 4,107 MBq/m$^2$ (111 mCi/m$^2$) of $^{131}$I-radretumab (~4.2 mg of protein). Although the calculation of provisional doses derived from dosimetric $^{131}$I-L19SIP administration has been reported (34, 35), here we describe a methodology to accurately determine the expected radretumab RIT doses to the bone red marrow, lesions, and healthy organs after dosimetric administration of $^{124}$I-L19SIP, which was applied to 6 patients in the above-mentioned trial. The study not only indicates that immuno-PET with $^{124}$I-labeled L19SIP allows the determination of accurate dosimetries for radioimmunotherapeutic treatment with $^{131}$I-labeled L19SIP, but it also identifies an unsuspected variability of antibody-uptake in different lesions, even within the same patient.

## Materials and Methods

### Patient population

The dosimetric studies were conducted on 6 patients (3 male and 3 female) enrolled in the clinical trial EudraCT no. 2009-013002-13 at Azienda Ospedaliera Papa Giovanni XXIII (Bergamo, Italy). Brain metastases were originating from non–small cell lung cancer ($n = 3$) or breast carcinoma ($n = 3$). All enrolled patients (or their legally acceptable representatives, when applicable) signed an informed consent form before being admitted to the study. The study was conducted in accordance with the Declaration of Helsinki, and was approved by the Italian national competent authority and the hospitals' ethic committees. The trial is registered in http://clinicaltrials.gov/ with the code NCT01125085.

### Patient eligibility and protocol design

Patient's eligibility for the therapeutic dose was based on the provisional dose to the bone red marrow (<2 Gy) and on the ratio of the $^{124}$I activity concentration in the cerebral metastases as compared with healthy brain (threshold: ratio > 4) obtained during the diagnostic phase. The therapeutic dose of $^{131}$I-L19SIP was established on the basis of the patient's body surface area calculated according to Du Bois and colleagues (36). Both for the diagnostic and the therapeutic dose, radiolabeled antibody preparation was administered by slow infusion over 10 minutes.

### L19SIP antibody and radiolabeling

L19SIP (Philogen S.p.A) was radioiodinated at Azienda Ospedaliera Papa Giovanni XXIII, using a modified chloramine-T method, as described previously (34, 35). Briefly, 4 mg of L19SIP were labeled with about 370 MBq of $^{124}$I-iodide [produced by the Advanced Center Oncology Macerata (ACOM), Montecosaro, Macerata, Italy) or 7.4 GBq of $^{131}$I-iodide (GE Healthcare; about 25 mg of chloramine-T for 4 mg of L19SIP; 3-minute reaction time) and purified with a Hiprep 26/10 Desalting Column (GE Healthcare). Administration occurred within 2 hours after

Downloaded from http://aacrjournals.org/cancerimmunolres/article-pdf/1/2/134/2342431/134.pdf by guest on 21 May 2022

labeling. The chloramine-T and Iodogen methods have been shown to yield comparable results for the radioiodination of whole mouse IgGs (37). In our hands, radioiodination via chloramine-T using a reductant to stop reactions consistently yielded high radioisotope incorporation rates without compromising immunoreactivity of the L19SIP antibodies.

Activities of $^{124}$I and $^{131}$I were measured using a calibrator CAPINTEC CRC-15PET. For each patient, 3 separate labeling reactions were carried out (one with $^{124}$I for the diagnostic dose and 2 others with $^{131}$I for the therapeutic dose, as a single reaction is insufficient to produce the necessary 7.4 GBq of $^{131}$I-L19SIP). The mean specific activities of the $^{124}$I- and $^{131}$I-labeled protein were 51 MBq/mg (range, 44–56 MBq/mg) and 1,705 MBq/mg (range, 1,517–2,171 MBq/mg), respectively. The mean radiochemical yield was 72% (range, 55%–82%); the mean radiochemical purity was 98% (range, 95%–99%); and the mean immunoreactivity was 93% (range, 86%–99%).

### Calibration of PET/CT

During the diagnostic phase with $^{124}$I-L19SIP, patients underwent a series of PET/CT assessments (Siemens Biograph 6 HiRez), conducted usually at 1, 4, 24, 48, and 96 hours after administration. Total body scans were acquired with 4 minutes per bed position, whereas brain scans were registered using one single bed position for 20 minutes. These investigations were carried out to determine the course of the activity in the lesions and in the various organs as a function of time.

Quantitative data are highly influenced by partial volume effect (PVE), especially for small lesions with linear dimensions comparable with the PET spatial resolution. A specific calibration of the PET scanner for $^{124}$I is therefore mandatory and was conducted using the National Electrical Manufacturers Association (NEMA) International Electrotechnical Commission (IEC) Body Phantom (Data Spectrum Corporation). The volume of the 6 spheres was determined by weighing each with a precision scale before and after filling with distilled water. The 6 spheres, with volumes of 0.57, 1.15, 2.60, 5.56, 11.52, and 26.95 cm$^3$, respectively, were then filled with a $^{124}$I solution of ca. 40 kBq/mL.

For each sphere, we determined the recovery coefficient, defined as the ratio of the measured and the actual activity concentration inserted into the sphere. The PET-derived activity concentration was defined using the segmentation method with threshold giving the real volume of the inner part of the sphere. This calculation was carried out for 4 different signal to background (S:B) ratios (38) equal to infinite (absence of background activity), 9, 5, and 3 (see Fig. 1A). The course of recovery coefficients as a function of the sphere volume (represented in Fig. 1B) was fitted for each S:B ratio as suggested by Jentzen and colleagues (38).

### Bone red marrow dose

The method based on the Medical Internal Radiation Dose (MIRD) formalism described in the European Association of Nuclear Medicine (EANM) guidelines (39, 40) was used to calculate the dose to the bone red marrow.

The value of activity concentration cumulated in the patient's blood $[\tilde{A}_{Bl}]$, which was used to calculate the contribution of self-irradiation to the bone red marrow dose, was determined by conducting a series of activity measurements in blood samples. To estimate the cross-absorbed dose to the bone red marrow from the activity in the body, the value of the cumulated activity in the total body $\tilde{A}_{TB}$ was determined with a series of residual activity in the whole body measurements. Both blood sampling and whole body measurements were typically conducted at 0.5, 4, 24, 48, 72, and 96 hours after administration.

### Measurement of activity concentration in the blood

Blood samples were collected in heparinized vials. Activity concentration in the blood was determined by γ-spectrometry, using a HPGe detector (EG&G ORTEC).

The γ-peak at 602.7 keV (intensity 62.9%) was used for the diagnostic phase with $^{124}$I, and the γ-peak at 364.5 keV (intensity 81.5%) of $^{131}$I was used for the posttherapy phase. To minimize statistical error, acquisition time for each sample was at least 10 minutes, to obtain a net peak area greater than $10^4$ counts. Two different measuring geometries were used for the diagnostic phase with $^{124}$I and the therapeutic phase with $^{131}$I to prevent high dead time values during the posttherapy blood sample analysis.

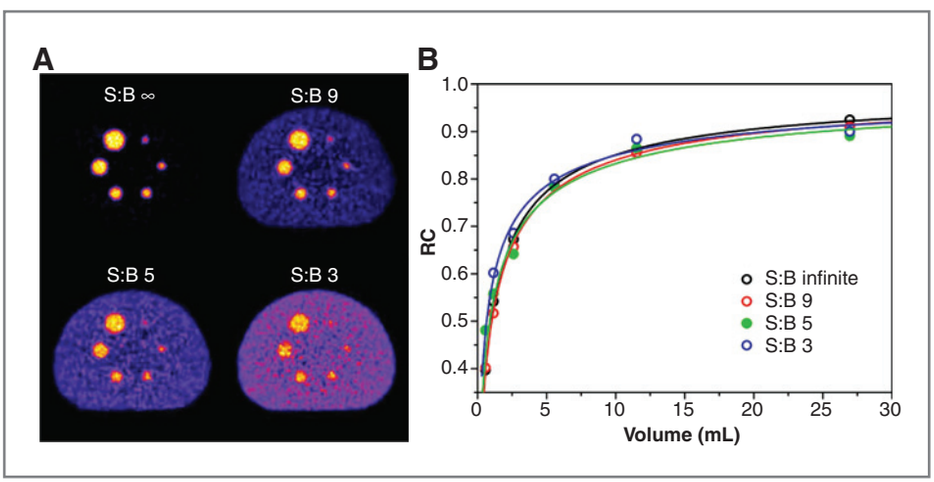


Figure 1. $^{124}$I PET/CT calibration. A, NEMA IEC Body Phantom PET acquisitions with $^{124}$I for spheres to background activity concentration ratios equal to infinite, 9, 5, and 3, conducted to obtain the recovery coefficients (RC; see Materials and Methods) for dosimetric calculations. B, course of the recovery coefficients as a function of sphere volume represented for different S:B concentration ratios.

Downloaded from http://aacrjournals.org/cancerimmunolres/article-pdf/1/2/134/2342431/134.pdf by guest on 21 May 2022

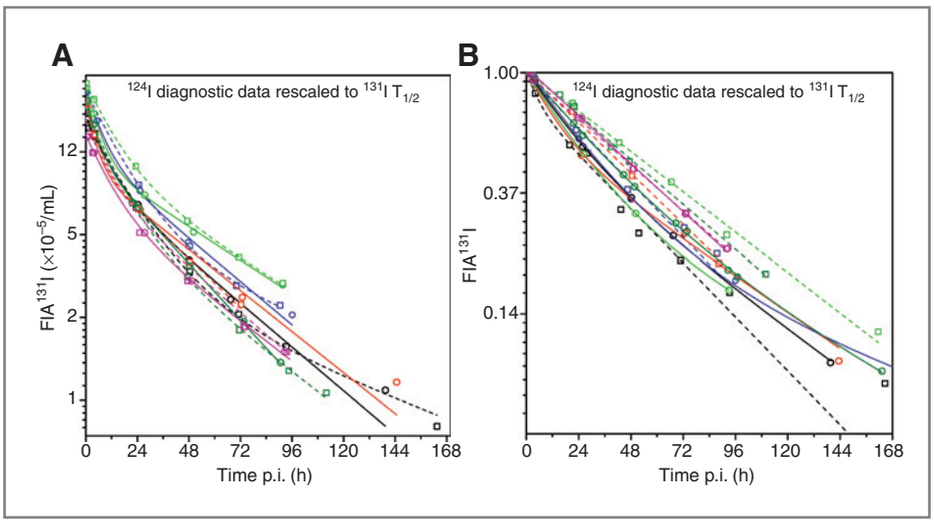


**Figure 2.** Bone red marrow dosimetry. A, time course of FIA/mL $^{131}$I in the blood of patients during the diagnostic (solid lines) and posttherapy phase (dashed lines). B, time course of FIA ($^{131}$I) in the body of patients during the diagnostic and posttherapy phase. $^{124}$I diagnostic data are rescaled to $^{131}$I half time. Different colors refer to different patients.

To avoid unnecessary manipulation of blood samples, the efficiency of the HPGe detector was calibrated as a function of the blood volume present in the vials. The blood mass of samples (usually 1.5–2.0 g) was determined by weighing the vials before and after blood draw using a precision scale. The detection efficiency for the γ-peak being considered was determined on the basis of the blood volume, calculated by dividing the mass by blood density (1.06 g/mL).

The fraction of injected activity (FIA) per mL of blood was calculated as the activity concentration at the moment of blood sampling divided by the activity administered to the patient.

The dose of interest to the bone red marrow obtained during the diagnostic phase is used for $^{131}$I administration. All FIA/mL values obtained during the diagnostic phase were corrected to account for the different half-lives of $^{124}$I and $^{131}$I.

Data related to the FIA/mL as a function of time passed from administration to blood sampling (Fig. 2A) were fitted with a biexponential function for the successive calculation of $[\tilde{A}_{\mathrm{Bl}}]$.

### Measurement of residual activity in the patient

To determine the cumulated activity $\tilde{A}_{\mathrm{TB}}$ in each patient, residual activity was measured at various time points after administration using a LaBr scintillator (Canberra InSpector 1000 with IPROL-1 probe). The residual activity was estimated as the net area of the γ-peak at 602.7 keV for the diagnostic and at 364.5 keV for the posttherapy phase. The probe measurements were made at a distance of at least 3 m from the patient, the acquisition time was chosen to have a peak net area of at least 10,000 counts, and the geometric mean was made between anterior and posterior acquisition. The first measurement was usually conducted within 30 minutes after drug administration, before first voiding. The result of this first measurement, corrected by the decay of the nuclide, was normalized to the activity injected into the patient. The measurements conducted during the diagnostic phase with $^{124}$I were corrected for the different half-life to obtain the residual activity expected for the $^{131}$I administration. Experimental data were fitted using a mono- or biexponential function for the successive calculation of the cumulated activity $\tilde{A}_{\mathrm{TB}}$ (Fig. 2B).

### Dose to lesions

Lesion volumes were determined on the basis of magnetic resonance or computed tomography (CT) scans using contrast agents, conducted few days before the PET studies. The mean volume of lesions for which it was possible to assess a dosimetric evaluation was 11.2 cm$^3$ (range, 0.4–40.9).

The lesion activity concentration was determined as the average activity in the volume defined by a volumetric region of interest (VROI) obtained using the segmentation method with threshold giving the real volume of the lesion.

The course of FIA as a function of time from administration was determined for each lesion. The course of activity concentration shows an uptake phase followed by a slower washout period. Experimental data were generally well fitted with a biexponential function $\mathrm{FIA}(t) = A \cdot e^{-b \cdot t} - C \cdot e^{-d \cdot t}$.

From this fit, the cumulated activity in the single lesion $\tilde{A}_{\mathrm{les}}$ was determined. The dose to the lesion was calculated by multiplying $\tilde{A}_{\mathrm{les}}$ with the $S$ factor of the MIRD model. This factor was derived from the spheres $S$ factors of the OLINDA/EXM software (41). $S$ factors for intermediate volumes compared with the ones provided by the software were determined from the fit with the following function $S = a \cdot m^b$, where $m$ is the sphere mass.

### Dose to healthy organs

The course of activity in various organs as a function of time (see Fig. 4B) was determined from the CT images of the PET/CT [regions of interest (ROI) were drawn on the organ of interest as visualized by the CT component of the PET/CT scan]. The activity in the organ was calculated by multiplying the VROI concentration with the VROI volume, without applying the PVE correction, except for the thyroid. The residence times in various organs were determined as the integral of the function fitting the FIA data into the OLINDA/EXM software

Downloaded from http://aacrjournals.org/cancerimmunolres/article-pdf/1/2/134/2342431/134.pdf by guest on 21 May 2022

for the successive calculation of dose to healthy organs. The OLINDA/EXM software was used with its standard phantoms. Residence times were calculated for the following organs: brain, liver, lungs, heart, spleen, thyroid, and kidneys.

### Statistical analysis

All statistical analyses were conducted using the statistical software SAS version 9.2 (SAS Institute).

## Results

### Calibration of PET/CT

The PET scanner was calibrated for $^{124}$I to quantify the activity present at each time point in the lesions. This calibration was necessary especially for small lesions for which PVE is most severe (see Materials and Methods). Using the IEC Body Phantom, recovery coefficients were determined as a function of the sphere volume for different S:B ratios (38).

Figure 1A shows $^{124}$I phantom images for S:B ratios equal to infinite, 9, 5, and 3, representing the loss of counts with decreasing sphere dimension due to PVE. Data were fitted using the equation described in ref. 38, resulting in the graph depicted in Fig. 1B. No significant differences were observed among the recovery coefficients obtained with different S:B ratios.

### Dose to bone red marrow

The calculation of the expected bone red marrow dose is an essential part of the dosimetric evaluation, as the bone red marrow is considered to be the dose-limiting organ for RIT applications. The dose is a function of the amount of radioactivity delivered by the antibody directly to the bone red marrow, and the contribution stemming from radioactivity in neighboring tissues.

The course of FIA/mL as a function of time in the blood of patients is depicted in Fig. 2A, which shows experimental data from samples obtained during the diagnostic and the therapeutic phases of the study. To correct for the different half-lives of the 2 radioiodine isotopes, the $^{124}$I data have been adjusted to the $T_{1/2}$ of $^{131}$I. In all cases, the blood clearance profiles are well described using a biexponential function characterized by a more rapid component with an average $T_{1/2}$ of 7 hours and a slower component with a $T_{1/2}$ of 39 hours. The maximum FIA/mL obtained by extrapolating the data to $t = 0$ was $2.2 \times 10^{-4}$. The self-dose component to the bone red marrow $D_{\mathrm{RM}\leftarrow\mathrm{RM}}$ was 0.117 Gy/GBq. The self-irradiation component of the bone red marrow was similar among various patients. Furthermore, the interpatient difference between the provisional dose obtained with $^{124}$I and the effective posttherapy dose with $^{131}$I was analyzed using a paired $t$ test and it was found not to be statistically significant ($P = 0.1653$).

The experimental data were further fitted using a mono-exponential function. In this case, the effective $T_{1/2}$ (again very similar among the various patients) resulted in an average value of 17 hours, which is higher than previously reported (42).

Figure 2B shows the time course of residual FIA (i.e., the component stemming from radioactivity accumulated in neighboring tissues) in patients after the diagnostic and therapeutic administration. Also in this case, data for the diagnostic phase of the study were rescaled to $T_{1/2}$ of $^{131}$I. For the diagnostic phase, data were well described using a biexponential function characterized by a more rapid component with an average $T_{1/2}$ of 18 hours and a slower component with a $T_{1/2}$ of 77 hours. In case of posttherapy data, a better fit was achieved using a mono-exponential function. The mono-exponential fit led to an average effective $T_{1/2}$ of 38 hours. The dose component to the bone red marrow due to the activity in the rest of the body $D_{\mathrm{RM}\leftarrow\mathrm{RB}}$ resulted in 0.089 Gy/GBq. The difference between the provisional $^{124}$I dose and the effective $^{131}$I dose is not statistically significant ($P = 0.9355$).

Overall, the average provisional dose to the bone red marrow from the diagnostic phase was 0.201 Gy/GBq, whereas the effective posttherapy dose was 0.210 Gy/GBq. The average calculated dose to the bone red marrow for administration of up to 7.4 GBq was therefore always below the 2 Gy threshold of the inclusion criteria. In general, there was an excellent match (within 5%) between provisional and effective $D_{\mathrm{RM}}$ for each patient.

### Radioactive doses to tumor lesions and to healthy organs

We have studied brain and extracranial lesions in 6 patients. In all lesions, we observed high 2-deoxy-2-[$^{18}$F]fluoro-D-glucose (FDG) uptake [mean standardized uptake value (SUV) of about 8] usually associated with high $^{124}$I-L19SIP uptake. In most cases, PET scans obtained 24 hours after administration of $^{124}$I-L19SIP could accurately detect extracranial lesions and brain metastases (Fig. 3). The comparison of Fig. 3D and E shows that image quality and resolution was highly superior with $^{124}$I-L19SIP immuno-PET procedures, as compared with dosimetric single photon emission computed tomography (SPECT) scans obtained with $^{131}$I-L19SIP (34).

The time course of FIA in brain and extracranial lesions can be described with an uptake phase followed by a slower washout (Fig. 4A). The maximal uptake value, obtained by fitting the data with function $\mathrm{FIA}(t) = A \cdot e^{-b \cdot t} - C \cdot e^{-d \cdot t}$, was on average reached after about 22 hours and showed a high variability from lesion to lesion, ranging from $2.95 \times 10^{-5}$ to $9.63 \times 10^{-3}$. The variability included lesions from the same patient (see for example those indicated by an asterisk). Taking into account the estimated mass of the lesions, the maximal value of injected dose (ID)%/g of tissue was found to be within a range between 0.0009% and 0.0356% (for the liver lesion of Fig. 3A and B).

All brain lesions for which a dosimetric evaluation was possible had an elevated activity concentration ratio between lesions and healthy brain, which was a consequence of the lower activity observed in the brain compared with other normal organs (Fig. 4B). S:B resulted in an average of 38 (range, 9–83), in line with an eligibility threshold for the therapeutic dose of $C_{\mathrm{les}}/C_{\mathrm{bkg}} > 4$.

The dose to the lesions ($D_{\mathrm{les}}$) was calculated by multiplying the integral of FIA($t$) by the $S$ factor (determined as a function of the lesion mass described in the Materials and Methods) and by the administered activity. The dose to the lesion per administered activity unit averaged 0.38 Gy/GBq (range, 0.10–1.37 Gy/GBq) and 1.41 Gy/GBq (range, 0.15–5.38 Gy/GBq)

Downloaded from http://aacrjournals.org/cancerimmunolres/article-pdf/1/2/134/2342431/134.pdf by guest on 21 May 2022

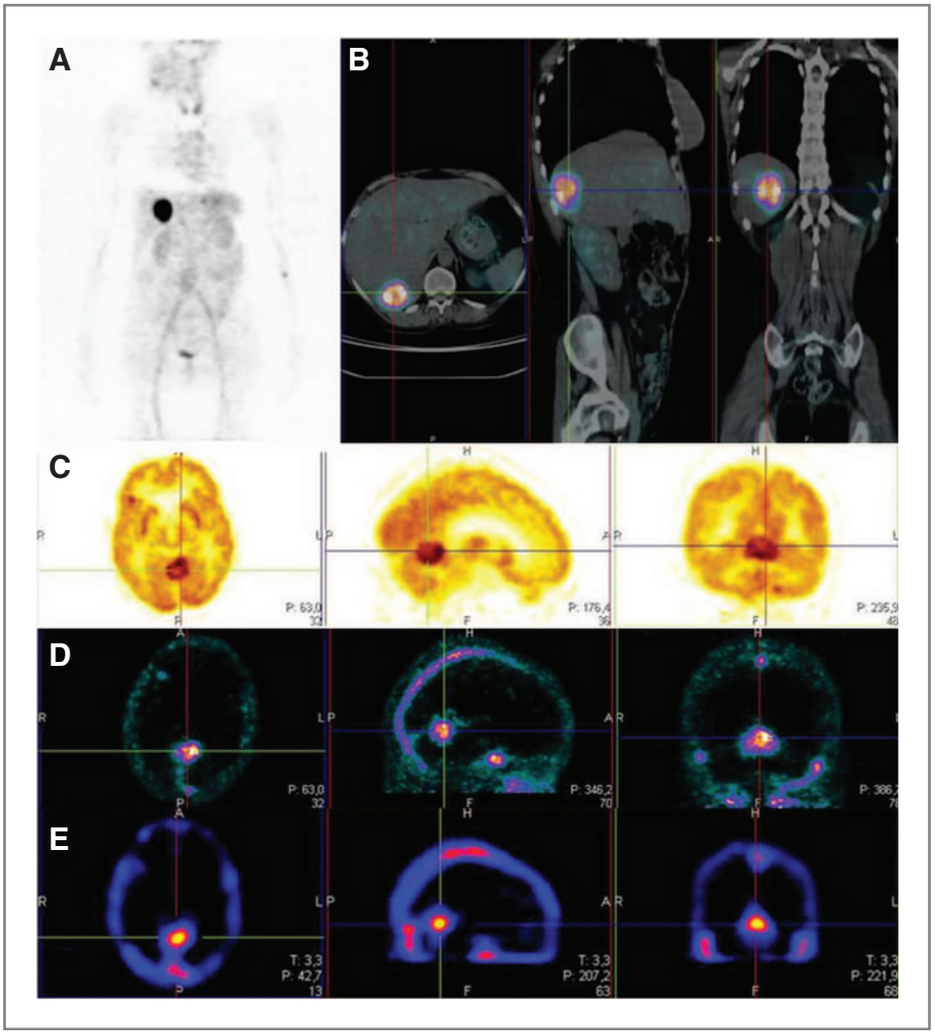


Figure 3. Examples of imaging data in patients. A, $^{124}$I-L19SIP PET image 24 hours p.i., showing a hepatic lesion with high antibody uptake. The corresponding transaxial, sagittal, and coronal projections PET/CT fusion images are depicted in B. C, FDG PET image of a lesion in the cerebellar region, visible despite the high metabolic uptake of glucose in the brain (transaxial, sagittal, and coronal projections); the corresponding PET images stemming from the diagnostic phase with $^{124}$I-L19SIP (24 hours p.i.) and SPECT images posttherapy from the use of $^{131}$I-L19SIP (24 hours p.i.) are depicted in D and E, respectively.

for brain metastases and extracranial lesions, respectively (Table 1). By multiplying these results by the administered activity to single patients during the therapeutic phase, average doses of 2.4 Gy (range, 0.7–8.1 Gy) and 7.3 Gy (range, 1.1–35.8 Gy) were obtained for brain metastases and extracranial lesions, respectively.

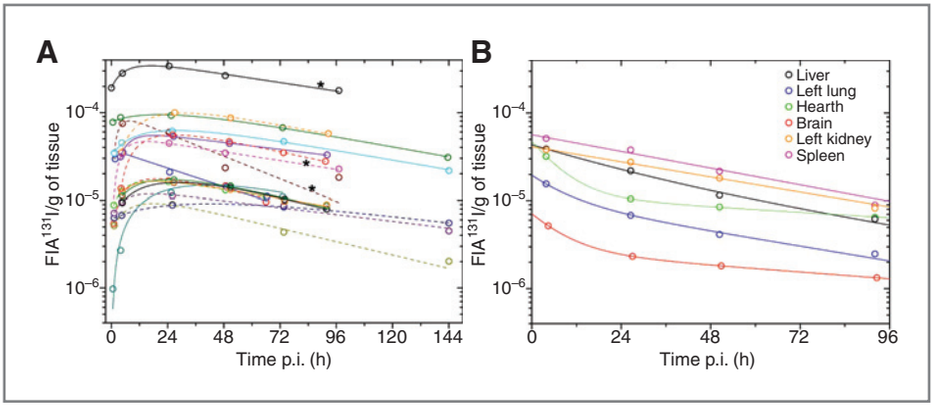


Figure 4. Lesions and healthy organs dosimetry. A, time course of FIA/g of tissue in selected brain lesions (dotted lines) and extracranial metastases (continuous lines) of all 6 patients. *, values for extracranial (liver) and brain lesions measured in the same patient. B, FIA/g of tissue time course in various organs from one patient. The $^{124}$I diagnostic values have been rescaled to match the physical half-life of $^{131}$I (8 days). The profiles thus represent an underestimate of the antibody residence on the lesion, as they contain an exponential component for the decay of the radionuclide.

Downloaded from http://aacrjournals.org/cancerimmunolres/article-pdf/1/2/134/2342431/134.pdf by guest on 21 May 2022

**Table 1.** Estimated doses to healthy organs, brain lesions, and extracranial metastases

| Organ/lesion | $D_{mean}$, Gy/GBq | Range, Gy/GBq |
|---|---|---|
| Adrenals | 0.192 | 0.153–0.229 |
| Brain | 0.076 | 0.064–0.086 |
| Breasts | 0.142 | 0.113–0.173 |
| Gall bladder wall | 0.194 | 0.158–0.232 |
| Lower large intestine wall | 0.178 | 0.144–0.221 |
| Small intestine | 0.178 | 0.149–0.213 |
| Stomach wall | 0.178 | 0.143–0.218 |
| Upper large intestine wall | 0.182 | 0.147–0.225 |
| Heart wall | 0.205 | 0.107–0.318 |
| Kidneys | 0.553 | 0.397–0.791 |
| Liver | 0.297 | 0.229–0.346 |
| Lungs | 0.340 | 0.224–0.293 |
| Muscle | 0.157 | 0.127–0.193 |
| Ovaries | 0.204 | 0.188–0.224 |
| Pancreas | 0.195 | 0.156–0.235 |
| Bone red marrow | 0.201 | 0.168–0.256 |
| Osteogenic cells | 0.326 | 0.257–0.411 |
| Skin | 0.132 | 0.106–0.163 |
| Spleen | 0.297 | 0.172–0.413 |
| Testes | 0.133 | 0.124–0.143 |
| Thymus | 0.169 | 0.133–0.204 |
| Thyroid | 2.648 | 0.807–5.650 |
| Urinary bladder wall | 0.168 | 0.142–0.201 |
| Uterus | 0.202 | 0.187–0.222 |
| Total body | 0.171 | 0.138–0.206 |
| Effective dose | 0.315 | 0.220–0.481 |
| Brain lesions | 0.376 | 0.099–1.370 |
| Extracranial lesions | 1.408 | 0.153–5.380 |

NOTE: The dose of radioactivity to the various organs (normalized per GBq of administered $^{131}$I-labeled antibody) was calculated as described in the Materials and Methods. Please note the large range of values in the brain and extracranial lesions, which are in stark contrast with the extremely narrow range observed for the normal organs. The high variability observed for the thyroid reflects a poor compliance of patients for their premedication with Lugol solution during the diagnostic phase of the study.

The radioactivity dose in normal organs was uniform among different patients (Table 1). The complete $^{124}$I-dosimetry to healthy organs is reported in the Supplementary Table S1. Only the thyroid showed a heterogeneous behavior among patients. This result might be explained by 3 of 6 patients not strictly following the thyroid blocking therapy prescribed by the nuclear medicine physician. In some cases, an increase in uptake to the thyroid was observed up to 96 hours after administration, and this led to high dose estimates for the thyroid. A better compliance was enforced before the therapeutic treatment with $^{131}$I-L19SIP (data not shown).

The radioactivity doses to the lesions, particularly to the extracranial metastases, were generally higher compared with normal organs (Table 2). However, the tumor:organ ratios (except for the brain) typically ranged between 0.5 and 20:1 at 24 hours p.i. (Fig. 4), suggesting that vascular permeability at the neoplastic site or total antigen density may contribute to the efficiency of the tumor targeting process.

## Discussion

There is considerable interest in measuring the efficiency of the tumor-targeting process of "armed" versions of anticancer antibodies (e.g., antibodies coupled with drugs, cytokines, or radionuclides), as preferential localization at the neoplastic site is expected to correlate with improved therapeutic outcome. The need for dosimetric studies is particularly important for RIT applications, not only to assess whether the radioactivity dose on the tumor is sufficient to yield a therapeutic benefit, but also to evaluate the potential toxicity to the bone red marrow and other critical organs.

Several studies have described the use of antibody-based imaging techniques to determine the feasibility of a subsequent RIT, (reviewed in ref. 43). We have recently reported the development of the fully human radiolabeled antibody product $^{124}$I-L19-SIP, which is ideally suited for immuno-PET imaging and dosimetric calculations before therapeutic intervention with $^{131}$I-L19SIP RIT (33). In our view, the combination of the chosen antibody format (SIP), isotope ($^{124}$I), and detection technique (immuno-PET) offers unique advantages over other existing approaches. The L19 antibody in SIP format has been shown to display superior dosimetric and therapeutic properties in mouse models of cancer, compared with the corresponding $(scFv)_2$ and IgG1 format counterparts (27). The $^{124}$I isotope has a physical half-life (100.2 hours), which matches well with the biologic half-life of proteins *in vivo* (Figs. 2 and 4; Table 1). Our results are consistent with those published by Wu and colleagues, who showed the advantages of using antibodies in mini-antibody format (functionally equivalent to SIP) and $^{124}$I as a PET radionuclide (44, 45).

The $^{124}$I-L19SIP product seems to be more stable than other radiohalogens, such as $^{76}$Br-L19SIP (46), and it displays a lower accumulation in critical organs (liver, spleen, and kidney) compared with radiometals (32). The identical chemical nature of the radioisotope used for immuno-PET ($^{124}$I) and for therapy ($^{131}$I) facilitates the determination of meaningful provisional therapeutic dosimetries. Immuno-PET methods allow high-resolution imaging and they seem to be superior to conventional SPECT procedures with $^{131}$I-labeled antibody preparations (Fig. 3). Although limited by the small number of patients, the work presented here suggests that immuno-PET imaging with $^{124}$I-labeled L19SIP could accurately predict the doses delivered to tumor lesions versus healthy organs by a subsequent therapeutic $^{131}$I-labeled L19SIP (radretumab) administration in cancer patients with brain metastasis.

$^{124}$I-L19SIP may find broad application for diagnostic imaging of cancer patients with cerebral and extracranial lesions. The use of a germanium detector to determine the activity in blood samples and a lanthanum bromide detector to measure the residual activity in the whole body proved to be a reliable method to assess the radioactivity dose to the bone red marrow, which provides an excellent agreement between the

Downloaded from http://aacrjournals.org/cancerimmunolres/article-pdf/1/2/134/2342431/134.pdf by guest on 21 May 2022

**Table 2.** Estimated doses to individual lesions

| Patient | Lesion | Mass g | Avg. dose Gy/GBq | Avg. dose Gy |
|---|---|---|---|---|
| 1 | Brain, left frontal | 22.8 | 0.20 | 1.48 |
| | Brain, right occipital | 23.1 | 0.24 | 1.75 |
| | Lung, right upper lobe | 0.8 | 0.15 | 1.11 |
| 2 | Brain, cerebellar vermis | 13.7 | 0.66 | 4.41 |
| | Brain, left lower temporomedial | 0.4 | 0.43 | 2.83 |
| | Liver | 27.0 | 5.38 | 35.84 |
| 3 | Brain, right anterior frontal | 7.0 | 0.22 | 1.61 |
| | Brain, left central frontal | 3.5 | 0.10 | 0.73 |
| | Brain, right nuclear | 2.5 | 0.21 | 1.55 |
| | Skull, left occipital theca | 4.0 | 0.98 | 7.24 |
| | Pelvis | 8.0 | 1.46 | 10.77 |
| | Lung | 34.1 | 0.18 | 1.34 |
| 4 | Brain, left cerebellar | 2.5 | 1.37 | 8.15 |
| | Liver | 40.9 | 1.01 | 5.98 |
| 5 | Brain, posterior frontal | 1.8 | 0.45 | 2.65 |
| 6 | Brain, left frontal operculum | 5.8 | 0.21 | 1.25 |
| | Brain, left posterior frontal | 3.2 | 0.19 | 1.12 |
| | Brain, right frontal coronal | 2.5 | 0.23 | 1.38 |
| | Vertebra | 10.0 | 0.69 | 4.11 |

diagnostic phase and the effective posttherapy doses (Fig. 2). Schwarz and colleagues (15) published dosimetry studies based on PET/CT of 2 different $^{124}$I-labeled monoclonal IgG1 antibodies (cG250 and huAe33), in which values of the self-dose to bone red marrow were slightly higher than those recorded in the present work. The different format of the antibody used here (SIP) could explain the observed differences, as conventional blood- or plasma-based dosimetry might overestimate bone red marrow doses for molecules smaller than intact IgGs, and with faster kinetics (15).

The bone red marrow dose was about 0.2 Gy/GBq and always lower than 2 Gy for the administered activities, suggesting that doses up to 7.4 GBq can be injected without compromising the blood building system in the long term. These findings were in line with the clinical finding that doses of $^{131}$I-labeled L19SIP up to 9.3 GBq could be safely administered to patients with cancer (42; manuscript in preparation).

Other L19-based immunotherapeutics are currently being developed clinically (L19-IL2 and L19-TNF) and have shown good tolerability and promising first signs of activity in cancer patients with metastases (47, 48). In the future, PET scans with $^{124}$I-L19SIP described here may be useful to preselect patients who are ideally suited to receive treatment with L19-based immunocytokines, based on the observation of preferential antibody uptake in tumor lesions. These experimental strategies are motivated by the observation of rather large variations of tumor-targeting efficiency among lesions and among patients (Fig. 4 and Table 1). Very recently, immuno-PET imaging and dosimetric studies have been conducted with a different monoclonal antibody (girentuximab), labeled with $^{124}$I or with other radionuclides (9, 10, 49). Girentuximab is a chimeric monoclonal antibody, specific to carbonic anhydrase IX, one of the best known markers for kidney cancer (50). Also in that case, dosimetric data revealed that a considerable variability of antibody uptake in the lesions could be observed, despite the fact that the antigen is strongly expressed in the majority of RCC lesions (51). Variations in local circulatory flow and vascular permeability of the individual lesions might partially explain the observed differences. These data reinforce the concept that immuno-PET studies may help guide pharmaceutical development, patient selection (e.g., by excluding patients with a majority of lesions which show poor uptake) and choice of antibody format (by pointing out the antibody format characterized by the highest residence time in the lesions) for therapeutic applications.

## Conclusion

We showed that administration of radretumab ($^{131}$I-labeled L19SIP), with an activity of 4,107 MB/m$^2$, is associated with a dose <2 Gy to the bone red marrow, which is the main organ at risk for this type of therapy. Immuno-PET imaging with $^{124}$I-labeled L19SIP represents a useful tool to predict doses delivered to tumor lesions and healthy organs by therapeutic administration of radretumab to patients. The image quality obtained with the immuno-PET procedure was superior to conventional SPECT scans with $^{131}$I-labeled antibody preparations, suggesting the applicability of $^{124}$I-labeled L19SIP for the determination of RIT dosimetries and for the noninvasive detection of L19 uptake in neoplastic lesions. Radretumab represents a well-tolerated therapeutic option, which has shown encouraging therapeutic results for treatment of patients with lymphoma (34, 35) or with brain metastases of various types of cancer, in combination with whole-brain external beam radiation (manuscript in preparation). The large

Downloaded from http://aacrjournals.org/cancerimmunolres/article-pdf/1/2/134/2342431/134.pdf by guest on 21 May 2022

variability of antibody uptake observed among different lesions and different patients suggests that immuno-PET studies may represent an important component for the future development of antibody-based therapeutic agents.

## Disclosure of Potential Conflicts of Interest

G. Elia is a consultant/advisory board member of Philogen S.p.A. D. Neri has ownership interest (including patents) and is a consultant/advisory board member of Philogen S.p.A. No potential conflicts of interest were disclosed by the other authors.

## Authors' Contributions

**Conception and design:** G.L. Poli, E. Trachsel, D. Neri
**Development of methodology:** G.L. Poli
**Acquisition of data (provided animals, acquired and managed patients, provided facilities, etc.):** G.L. Poli, C. Bianchi, G. Virotta, A. Bettini
**Analysis and interpretation of data (e.g., statistical analysis, biostatistics, computational analysis):** G.L. Poli, C. Bianchi, G. Virotta, A. Bettini, L. Giovannoni, A. Bruno
**Writing, review, and/or revision of the manuscript:** G.L. Poli, C. Bianchi, G. Virotta, A. Bettini, R. Moretti, E. Trachsel, G. Elia, L. Giovannoni, D. Neri, A. Bruno
**Administrative, technical, or material support (i.e., reporting or organizing data, constructing databases):** L. Giovannoni
**Study supervision:** G.L. Poli, G. Virotta, A. Bettini, D. Neri, A. Bruno

## Grant Support

Philogen S.p.A. financed the article-processing charge.

The costs of publication of this article were defrayed in part by the payment of page charges. This article must therefore be hereby marked *advertisement* in accordance with 18 U.S.C. Section 1734 solely to indicate this fact.

Received February 10, 2013; revised March 26, 2013; accepted March 30, 2013; published OnlineFirst May 20, 2013.

## References

1. Senter PD. Potent antibody drug conjugates for cancer therapy. Curr Opin Chem Biol 2009;13:235–44.
2. Steiner M, Neri D. Antibody-radionuclide conjugates for cancer therapy: historical considerations and new trends. Clin Cancer Res 2011; 17:6406–16.
3. Pasche N, Neri D. Immunocytokines: a novel class of potent armed antibodies. Drug Discov Today 2012;17:583–90.
4. Baeuerle PA, Reinhardt C. Bispecific T-cell engaging antibodies for cancer therapy. Cancer Res 2009;69:4941–4.
5. Kontermann RE. Antibody-cytokine fusion proteins. Arch Biochem Biophys 2012;526:194–205.
6. Marik J, Junutula JR. Emerging role of immunoPET in receptor targeted cancer therapy. Curr Drug Deliv 2011;8:70–8.
7. McCabe KE, Wu AM. Positive progress in immunoPET—not just a coincidence. Cancer Biother Radiopharm 2010;25:253–61.
8. van Dongen GA, Visser GW, Lub-de Hooge MN, de Vries EG, Perk LR. Immuno-PET: a navigator in monoclonal antibody development and applications. Oncologist 2007;12:1379–89.
9. Divgi CR, Uzzo RG, Gatsonis C, Bartz R, Treutner S, Yu JQ, et al. Positron emission tomography/computed tomography identification of clear cell renal cell carcinoma: results from the REDECT trial. J Clin Oncol 2013;31:187–94.
10. Smaldone MC, Chen DY, Yu JQ, Plimack ER. Potential role of (124)I-girentuximab in the presurgical diagnosis of clear-cell renal cell cancer. Biologics 2012;6:395–407.
11. Borjesson PK, Jauw YW, de Bree R, Roos JC, Castelijns JA, Leemans CR, et al. Radiation dosimetry of 89Zr-labeled chimeric monoclonal antibody U36 as used for immuno-PET in head and neck cancer patients. J Nucl Med 2009;50:1828–36.
12. Divgi CR, Pandit-Taskar N, Jungbluth AA, Reuter VE, Gonen M, Ruan S, et al. Preoperative characterisation of clear-cell renal carcinoma using iodine-124-labelled antibody chimeric G250 (124I-cG250) and PET in patients with renal masses: a phase I trial. Lancet Oncol 2007;8:304–10.
13. O'Donoghue JA, Smith-Jones PM, Humm JL, Ruan S, Pryma DA, Jungbluth AA, et al. 124I-huA33 antibody uptake is driven by A33 antigen concentration in tissues from colorectal cancer patients imaged by immuno-PET. J Nucl Med 2011;52:1878–85.
14. Pryma DA, O'Donoghue JA, Humm JL, Jungbluth AA, Old LJ, Larson SM, et al. Correlation of *in vivo* and *in vitro* measures of carbonic anhydrase IX antigen expression in renal masses using antibody 124I-cG250. J Nucl Med 2011;52:535–40.
15. Schwartz J, Humm JL, Divgi CR, Larson SM, O'Donoghue JA. Bone marrow dosimetry using 124I-PET. J Nucl Med 2012;53:615–21.
16. Chen G, Huynh M, Chen A, Fehrenbacher L, Gandara D, Lau D. Chemotherapy for brain metastases in small-cell lung cancer. Clin Lung Cancer 2008;9:35–8.
17. Eichler AF, Loeffler JS. Multidisciplinary management of brain metastases. Oncologist 2007;12:884–98.
18. Mintz A, Perry J, Spithoff K, Chambers A, Laperriere N. Management of single brain metastasis: a practice guideline. Curr Oncol 2007;14: 131–43.
19. Soffietti R, Ruda R, Mutani R. Management of brain metastases. J Neurol 2002;249:1357–69.
20. Soffietti R, Ruda R, Trevisan E. Brain metastases: current management and new developments. Curr Opin Oncol 2008;20:676–84.
21. Bezjak A, Adam J, Barton R, Panzarella T, Laperriere N, Wong CS, et al. Symptom response after palliative radiotherapy for patients with brain metastases. Eur J Cancer 2002;38:487–96.
22. Khuntia D, Brown P, Li J, Mehta MP. Whole-brain radiotherapy in the management of brain metastasis. J Clin Oncol 2006;24:1295–304.
23. Tsao MN, Lloyd N, Wong R, Chow E, Rakovitch E, Laperriere N. Whole brain radiotherapy for the treatment of multiple brain metastases. Cochrane Database Syst Rev 2006;3:CD003869.
24. Tsao MN, Lloyd NS, Wong RK, Rakovitch E, Chow E, Laperriere N. Radiotherapeutic management of brain metastases: a systematic review and meta-analysis. Cancer Treat Rev 2005;31:256–73.
25. Mohammadi AM, Recinos PF, Barnett GH, Weil RJ, Vogelbaum MA, Chao ST, et al. Role of Gamma Knife surgery in patients with 5 or more brain metastases. J Neurosurg 2012;117(Suppl):5–12.
26. Li J, Bentzen SM, Renschler M, Mehta MP. Regression after whole-brain radiation therapy for brain metastases correlates with survival and improved neurocognitive function. J Clin Oncol 2007;25: 1260–6.
27. Borsi L, Balza E, Bestagno M, Castellani P, Carnemolla B, Biro A, et al. Selective targeting of tumoral vasculature: comparison of different formats of an antibody (L19) to the ED-B domain of fibronectin. Int J Cancer 2002;102:75–85.
28. Neri D, Bicknell R. Tumour vascular targeting. Nat Rev Cancer 2005;5: 436–46.
29. Schliemann C, Wiedmer A, Pedretti M, Szczepanowski M, Klapper W, Neri D. Three clinical-stage tumor targeting antibodies reveal differential expression of oncofetal fibronectin and tenascin-C isoforms in human lymphoma. Leukemia Res 2009;33:1718–22.
30. Schliemann C, Neri D. Antibody-based vascular tumor targeting. Recent Results Cancer Res 2010;180:201–16.
31. Berndorff D, Borkowski S, Sieger S, Rother A, Friebe M, Viti F, et al. Radioimmunotherapy of solid tumors by targeting extra domain B fibronectin: identification of the best-suited radioimmunoconjugate. Clin Cancer Res 2005;11:7053s–63s.
32. Tijink BM, Neri D, Leemans CR, Budde M, Dinkelborg LM, Stigter-van Walsum M, et al. Radioimmunotherapy of head and neck cancer xenografts using 131I-labeled antibody L19-SIP for selective targeting of tumor vasculature. J Nucl Med 2006;47:1127–35.
33. Tijink BM, Perk LR, Budde M, Stigter-van Walsum M, Visser GW, Kloet RW, et al. (124)I-L19-SIP for immuno-PET imaging of tumour vasculature and guidance of (131)I-L19-SIP radioimmunotherapy. Eur J Nucl Med Mol Imaging 2009;36:1235–44.

Downloaded from http://aacrjournals.org/cancerimmunolres/article-pdf/1/2/134/2342431/134.pdf by guest on 21 May 2022

34. Erba PA, Sollini M, Orciuolo E, Traino C, Petrini M, Paganelli G, et al. Radioimmunotherapy with radretumab in patients with relapsed hematologic malignancies. J Nucl Med 2012;53:922–7.
35. Sauer S, Erba PA, Petrini M, Menrad A, Giovannoni L, Grana C, et al. Expression of the oncofetal ED-B-containing fibronectin isoform in hematologic tumors enables ED-B–targeted 131I-L19SIP radioimmunotherapy in Hodgkin lymphoma patients. Blood 2009;113:2265–74.
36. Du Bois D, Du Bois EF. A formula to estimate the approximate surface area if height and weight be known. 1916. Nutrition 1989;5:303–11.
37. Woltanski KP, Besch W, Keilacker H, Ziegler M, Kohnert KD. Radioiodination of peptide hormones and immunoglobulin preparations: comparison of the chloramine T and iodogen method. Exp Clin Endocrinol 1990;95:39–46.
38. Jentzen W, Weise R, Kupferschlager J, Freudenberg L, Brandau W, Bares R, et al. Iodine-124 PET dosimetry in differentiated thyroid cancer: recovery coefficient in 2D and 3D modes for PET(/CT) systems. Eur J Nucl Med Mol Imaging 2008;35:611–23.
39. Hindorf C, Glatting G, Chiesa C, Linden O, Flux G. EANM Dosimetry Committee guidelines for bone marrow and whole-body dosimetry. Eur J Nucl Med Mol Imaging 2010;37:1238–50.
40. Hindorf C, Linden O, Tennvall J, Wingardh K, Strand SE. Evaluation of methods for red marrow dosimetry based on patients undergoing radioimmunotherapy. Acta Oncol 2005;44:579–88.
41. Stabin MG, Sparks RB, Crowe E. OLINDA/EXM: the second-generation personal computer software for internal dose assessment in nuclear medicine. J Nucl Med 2005;46:1023–7.
42. Del Conte G, Erba PA, Fasolo A, Chiesa C, Grana C, Menssen H, et al. Radioimmunotherapy (RIT) with 131I-L19SIP in solid cancers (SC) and lymphoproliferative diseases: final results of the first human trial. J Clin Oncol 28:15s, 2010 (suppl; abstr 2523).
43. Barbet J, Bardies M, Bourgeois M, Chatal JF, Cherel M, Davodeau F, et al. Radiolabeled antibodies for cancer imaging and therapy. Methods Mol Biol 2012;907:681–97.
44. Olafsen T, Sirk SJ, Betting DJ, Kenanova VE, Bauer KB, Ladno W, et al. ImmunoPET imaging of B-cell lymphoma using 124I-anti-CD20 scFv dimers (diabodies). Protein Eng Des Sel 2010;23:243–9.
45. Knowles SM, Wu AM. Advances in immuno-positron emission tomography: antibodies for molecular imaging in oncology. J Clin Oncol 2012;30:3884–92.
46. Rossin R, Berndorff D, Friebe M, Dinkelborg LM, Welch MJ. Small-animal PET of tumor angiogenesis using a (76)Br-labeled human recombinant antibody fragment to the ED-B domain of fibronectin. J Nucl Med 2007;48:1172–9.
47. Johannsen M, Spitaleri G, Curigliano G, Roigas J, Weikert S, Kempkensteffen C, et al. The tumour-targeting human L19-IL2 immunocytokine: preclinical safety studies, phase I clinical trial in patients with solid tumours and expansion into patients with advanced renal cell carcinoma. Eur J Cancer 2010;46:2926–35.
48. Eigentler TK, Weide B, de Braud F, Spitaleri G, Romanini A, Pflugfelder A, et al. A dose-escalation and signal-generating study of the immunocytokine L19-IL2 in combination with dacarbazine for the therapy of patients with metastatic melanoma. Clin Cancer Res 2011;17:7732–42.
49. Povoski SP, Hall NC, Murrey DA, Sharp DS, Hitchcock CL, Mojzisik CM, et al. Multimodal imaging and detection strategy with 124 I-labeled chimeric monoclonal antibody cG250 for accurate localization and confirmation of extent of disease during laparoscopic and open surgical resection of clear cell renal cell carcinoma. Surgical Innov 2013;20:59–69.
50. Neri D, Supuran CT. Interfering with pH regulation in tumours as a therapeutic strategy. Nat Rev Drug Discov 2011;10:767–77.
51. Stillebroer AB, Zegers CM, Boerman OC, Oosterwijk E, Mulders PF, O'Donoghue JA, et al. Dosimetric analysis of 177Lu-cG250 radioimmunotherapy in renal cell carcinoma patients: correlation with myelotoxicity and pretherapeutic absorbed dose predictions based on 111In-cG250 imaging. J Nucl Med 2012;53:82–9.


Downloaded from http://aacrjournals.org/cancerimmunolres/article-pdf/1/2/134/2342431/134.pdf by guest on 21 May 2022